Article

Surveillance of Daughter Micronodule Formation is A Key Factor for Vaccine Evaluation Using Experimental Infection Models of Tuberculosis in Macaques.

Isabel Nogueira[1§], Martí Català [2,3,§], Andrew D. White[4], Sally A Sharpe[4], Jordi Bechini[1], Clara Prats[3], Cristina Vilaplana[5,6], Pere-Joan Cardona [5,6,7,8,*]

[1]Radiology Department, 'Germans Trias i Pujol' University Hospital, 08916 Badalona, Catalonia. Spain. inogueira. germanstrias@gencat.cat (I.N.), jbechini.germanstrias@gencat.cat (J.B.)

[2]Comparative Medicine and Bioimage Centre of Catalonia (CMCiB), Germans Trias i Pujol Research Institute (IGTP), 08916 Badalona, Catalonia, Spain. marticatalasabate@gmail.com (M.C.)

[3]Escola d'Enginyeria Agroalimentària i de Biosistemes de Barcelona Departament de Física, Universitat Politècnica de Catalunya (UPC)-BarcelonaTech, 08860 Castelldefels, Catalonia, Spain. clara.prats@upc.edu (C.P.)

[4]UK Health Security Agency, Porton Down, Salisbury SP4 0JG, UK. Andrew.white@pukhsa.gov.uk (A.D.W), sally.sharpe@ukhsa.gov.uk (S.A.S.)

[5]Unitat de Tuberculosi Experimental, Germans Trias i Pujol Research Institute (IGTP), 08916 Badalona, Catalonia, Spain. cvilaplana@gmail.com (C.V.)

[6]Centro de Investigación Biomédica en Red de Enfermedades Respiratorias (CIBERES), 28029 Madrid, Spain

[7]Microbiology Department, North Metropolitan Clinical Laboratory, 'Germans Trias i Pujol' University Hospital, 08916 Badalona, Catalonia. Spain. pj.cardona@gmail.com (P.-J.C.)

[8]Genetics and Microbiology Department, Universitat Autònoma de Barcelona, 08913 Cerdanyola del Vallès, Catalonia, Spain.

§ I.N. and M.C. have and equal contribution in the paper.

*Correspondence: pj.cardona@gmail.com

Abstract: Tuberculosis (TB) is still a worldwide major health problem and models using non-human primates (NHP) provide the most relevant approach for vaccine testing. In this study we have analysed CT images collected from cynomolgus and rhesus macaques, following exposure to ultra-low dose *Mycobacterium tuberculosis* (Mtb) aerosols, and monitored them for 16 weeks to evaluate the impact of prior intradermal or inhaled BCG-vaccination on the progression of lung disease. All lesions found (2553) have been classified according to their size and we have subclassified small micronodules (<4.4 mm) as 'isolated', or as 'daughter' when they are in contact with consolidation (described as lesions ≥ 4.5 mm). Our data links the higher capacity to contain Mtb infection in cynomolgus with the reduced incidence of daughter micronodules, thus avoiding the development of consolidated lesions and their consequent enlargement and evolution to cavitation. In the case of rhesus, intradermal vaccination has a higher capacity to reduce the formation of daughter. This study supports the 'Bubble Model' defined with the C3HBe/FeJ mice and proposes a new method to evaluate outcome in experimental models of TB in NHP based on CT images, which would fit a future machine learning approach to evaluate new vaccines.

Keywords: tuberculosis; BCG vaccine; aerosol vaccination; non-human primate; macaque; bubble model; computed tomography scanner

1. Introduction

 doi:10.20944/preprints202211.0529.v1

Understanding the dynamics of tuberculosis (TB) disease is essential for the design of better strategies against it, as TB is a cause of high morbidity and mortality worldwide. *Mycobacterium tuberculosis* (Mtb) infects about 10 million people every year and a quarter of humanity is estimated to be infected. Moreover, it has been the deadliest single infectious disease for decades, killing nearly 1.5 million people annually [1]. Unfortunately, this mortality has been overtaken by SARS-CoV-2 in 2020, a further consequence of which has been a devastating impact on TB Care resulting in an estimated additional half a million TB deaths, thus going back to a mortality level similar to that of 2010 [2,3]. Defeating TB is not yet a feasible goal in the short-term, but endeavours must continue to focus on the three cornerstones of prevention, early diagnosis and treatment, and advance the development of new vaccines, biomarkers and drugs with shorten protocols[4–6].

Mycobacterium tuberculosis is transmitted by aerosols which travel through the respiratory tract to reach the alveolar spaces, where it is able to multiply even within alveolar macrophages. The disease is developed due to the failure of the immune system to contain Mtb growth, and while the lungs are the most involved site (as the primary site of infection), disease can affect any organ. The infection can progress to cause serious pneumonia and cavitated lesions, which bring a poorer prognosis and generate both therapeutic challenges and higher transmission rates [7,8]. So, the analysis of pulmonary TB is fundamental because prophylactic strategies that concern lung involvement deliver a critical impact on morbidity and mortality.

The granuloma is the hallmark of the host response against Mtb infection, appearing as a characteristic round histologic structure ranging in size from 1-3 mm in diameter [9–12]. There are several studies that describe granuloma subtypes, mainly based on their cell proliferation, matrix quality and pattern distribution under microscope [9–11,13–16]. In the context of image analysis, granulomas are expected to profusely mineralize and thus be identifiable as calcified micronodules on CT scan images collected from macaques mainly from 20 weeks after experimental infection [11].

Vaccination is one of the essentials to control the disease. The Bacille Calmette-Guérin (BCG) vaccine is an attenuated strain of *Mycobacterium bovis* which was first used in 1921 and still plays a pivotal role in high endemic TB countries, despite low efficacy in some regions [17,18]. BCG has demonstrated protection against TB death and disseminated disease, especially against childhood tuberculous meningitis and miliary disease, but has also shown disparate results in the protection afforded to adults and pulmonary involvement [19–24]. Even though new vaccine candidates are in development [25–27], the centenary vaccine remains as the only licensed vaccine [1] and clinical trials are currently ongoing to explore the efficacy of BCG novel protocols, such as the use of alternative delivery routes like inhaled (or aerosolized)[28–32], or in revaccination regimens [33,34]

Investigation of prevention strategies and treatments depend on well characterized experimental animal models, to provide accurate, sensitive and reproducible methods to measure TB disease and to evaluate treatment outcomes. Mice and guinea pigs have been extensively used, but the most clinically relevant experimental models are provided by non-human primates (NHP) as they resemble humans in almost every aspect and mimic human physiological patterns. Macaques are widely reported to manifest the same TB disease as people do [35], also sharing comparable efficacy after BCG vaccination and chemotherapy [36–39]. It is worth emphasizing that investigation of BCG vaccination in macaques allows the exploration of the whole spectrum of the protection status seen in humans, as the vaccine confers a protective effect in cynomolgus macaques and limited protection in rhesus [28,29,40,41]. The model in rhesus macaques is the one that robustly reproduces active TB lesions [14,36,42–45]. In contrast, cynomolgus macaques reveal a greater similarity with the wide spectrum of outcomes that follow human-Mtb interaction, especially the Asian cynomolgus (with Indonesian and Chinese genotypes) which are better able to contain the progression of the infection, reflecting mainly a latent tuberculosis infection, and more limited progression towards active disease [14,15,29]. However, Mauritanian genotype cynomolgus macaques are more susceptible to TB disease, showing outcomes of TB infection more akin to those made by rhesus macaques [45,46]

One important consideration when designing experimental models is to use the route of natural infection and an optimal challenge dose that is sufficient to induce measurable disease, but not at a level that could overwhelm potentially protective effects induced by vaccination and confound the evaluation assessment [14,15,30,36,38,44,47]. The infection after experimental exposure to aerosols containing ultra-low dose inoculum has been demonstrated to closely resemble

 doi:10.20944/preprints202211.0529.v1

naturally-occurring Mtb exposure, causing disease-induced changes in the lung that can be monitored [14,48]. The evaluation method should be sensitive to allow the detection of subtle differences among prophylactic candidates.

Tuberculosis disease dynamics is not yet entirely understood. In fact, there is still not a canonical hypothesis to explain the progression from latent to active disease. Daughter lesions have already been described during active TB development, appearing near larger lesions, and being associated with the advance of local infection. The 'Bubble Model', firstly conceived by Prats *et al.*, 2016 [49] and, inspired by soap bubble formation together with previous concepts [5,49–53], hypothesized that progression to active TB was the consequence of the intensity of the inflammatory response in the initial micronodules, the induction of daughter micronodules around the initial nodule and the coalescence of all these lesions that cause the formation of a consolidated lesion, with cavitation capacity. However, this model was built on data obtained from the murine model with C3HeB/FeJ mice by Marzo *et al.* (2014) [54]. Supportive data obtained from the NHP model would endorse future confirmation in humans.

Image analysis plays a fundamental role in TB disease assessment. Chest X-ray was classically used for diagnosis and still remains a basic tool due to its widespread availability and sufficient sensitivity. Recently, high-quality diagnostic images like computed tomography (CT), positron emission tomography–computed tomography (PET-CT) and magnetic resonance imaging (MRI) have emerged. However, to our knowledge, there have been limited opportunities to characterize the development of Mtb-induced disease particularly the early events after infection. Scanning enables the collection of high quality data in a non-invasive way, allowing the examination of features of particular interest such as lung consolidations, nodules, micronodules (daughter and isolated), cavitation, tree-in-bud lesions and their distribution [5,11,59–61,46,48,49,54–58]. MRI scan is superior to gross examination in necropsy for the evaluation of lung lesion burden, and also allows the assessment of lesion volume and distribution [46,62]. PET-CT is especially useful for the detection of lesions with active TB metabolism, based on their high glucose demand, in contrast to latent or fibrotic forms which do not show activity. CT scanning allows the acquisition of high-quality images in a few seconds (notably faster than MRI and PET-CT), thus minimizing interference caused by respiratory motion, being also the most available and economical three-dimensional imaging technology. A score system for the estimation of TB burden disease in the NHP model based in CT images developed by Sharpe *et al*. (2018) [63] has been reported.

The aim of this study has been to evaluate the progression of Mtb infection in experimental NHP models through the spatial monitoring of the micronodules and the identification of consolidations with daughter micronodules as a tool to evaluate the efficacy of new vaccines.

2. Materials and Methods

2.1. Animals

Images were obtained from thirty-five alive macaques aged 3-4 years, thirteen cynomolgus macaques (*Macaca fascicularis*, of Indonesian genotype) and twenty-two rhesus macaques (*Macaca mulatta*, of Indian genotype) from established closed UK breeding colonies. The macaques were experimentally infected with *Mycobacterium tuberculosis* (Erdman strain K 01) ultra-low dose aerosol exposure as previously described (14). Groups were BCG-vaccinated via aerosol or intradermal injection with Danish strain 1331 (SSI, Copenhagen, Denmark) [13,14,28]. Animals were housed in compatible social groups, in accordance with the Home Office (UK) Code of Practice for the Housing and Care of Animals Used in Scientific Procedures (1989), now updated to Code of Practice for the Housing and Care of Animals Bred, Supplied or Used for Scientific Purposes, December 2014, and the National Committee for Refinement, Reduction and Replacement (NC3Rs), Guidelines on Primate Accommodation, Care and Use, August 2006 (NC3Rs, 2006).

 doi:10.20944/preprints202211.0529.v1

2.2. CT Images

We have analysed 123 computed tomography (CT) scans obtained from subjects enrolled in different studies [13,14,28] where sequential images were acquired from each macaque on three or four occasions during the post-infection period from the 3rd to the 16th week (**Suppl. Figure 1**). Further CT scans inspection showed the lung lobes to be separated by pleural fissures as well as bronchovascular bundles, thus presenting the same airway anatomy pattern seen in humans. The right lung is the largest and is composed of upper, middle, lower and infracardiac (or accessory or azygous) lobes, and the left lung is composed of upper, middle (or lingula) and lower lobes [64–68]. However, in our study, fissure for the middle left lobe was frequently incomplete or even absent.

Chest multidetector CT scans were obtained by using a 16 slice Lightspeed CT scanner (General Electric Healthcare, Milwaukee, WI, USA), from sedated subjects while free breathing. Technical parameters applied: tube voltage, 120kVp; tube current modulation, 100-150 mA. Reconstructions were made using a high spatial frequency algorithm and lung window at a slice thickness of 0.625mm. These technical parameters are extracted from the original animal experimental studies [13,14,28].

2.3. TB lung lesions analysis from CT images

CT scans were evaluated by a medical consultant radiologist with expertise in respiratory diseases blinded to vaccination status and clinical data. Images were then examined in Philips IntelliSpace Portal software (2015 Koninklijke Philips N.V.) by multiplanar reformatting axial, coronal and sagittal, and maximum intensity projection (MIP) to detect the smallest nodules. The Tumor Tracking tool from the mentioned software was used to analyse the volume and main axis of each lesion. We have used standard image descriptors, accepted and reproducible concepts from radiologic lexicon detailed on Fleischner Society Glossary [69] as well as in previous studies based on CT images [63].

A. Micronodule is a small solid lung nodule with smooth margins. We have considered all lesions with a maximum axis ranging from 1 to 4.4 mm (which equates to a maximum volume of 0.044cm^3). Their length mainly falls in the granuloma's size (1-3mm), but we also included rounded spherical lesions with a maximum axis under 4.5 mm, as they tended to be stable. In contrast, almost all lesions above 4.5 mm increased or showed an instable size. We have defined two subgroups: **a) Daughter micronodules**, found around consolidations, like satellites, that are presumably generated from that consolidated lesion [5,49,54]. They are located within an annular zone, where the amplitude of this circular crown corresponds to the consolidation's short axis; they were counted for each CT scan (**Figure 1**); **b) Isolated micronodules**, the ones independent or not associated with a consolidated lesion (**Figure 2**). The size and number of them were determined together within their bronchopulmonary segment.

B. Consolidation (also referred as consolidated lesion) is a pneumonic patch or necrotizing consolidative process which occupies and even destroys alveoli, and it is described in CT images as a soft tissue lesion within lung parenchyma showing irregular margins. Consolidations are large enough to be followed-up and carefully tracked over consecutive scans, and their axis (mm) and volume (cm^3) were measured (**Figure 3**). We have considered that these kinds of lesions modify their size over time and are equal or bigger than 4.5mm.

C. Cavitation corresponds to the appearance of gas within lung consolidations. It is described as a central radiolucency image, which matches with gas density, surrounded by soft tissue [8,57]. In addition, these lesions must have a greater size than the surrounding bronchial calibre, for avoiding misinterpretation with air bronchogram. It has been assessed qualitatively, being present (yes) or absent (no).

D. Pleural distance is defined as the distance between the margin of each consolidation to the closest pleura or fissure.

We have also determined the lung volume from each animal, using the COPD tool from the Philips IntelliSpace Portal software, which allowed the evaluation of the main airway and volume from both lungs separately.

 doi:10.20944/preprints202211.0529.v1

We also observed foci of bronchocentric pneumonia, detected as 'tree-in-bud' pattern in CT images, which is a common CT finding in active lung tuberculosis [58–61,70,71]. However, we did not include them in our analyses due to their lack of homogeneity and instability, which made them difficult to demarcate and to follow-up.

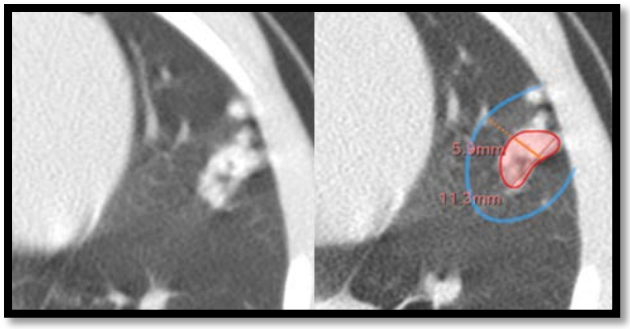

Figure 1. Consolidation with Daughter micronodules. Left picture shows original CT image from a lesion located in the inferior lingular bronchopulmonary segment at 11th week scan in an unvaccinated rhesus (RUV10). Right picture exposes that daughter micronodules are those situated within a surrounding area which has the same length as the consolidation's short axis. At same time, this figure exhibits the lesional complex consisting of a consolidation with daughter micronodules.

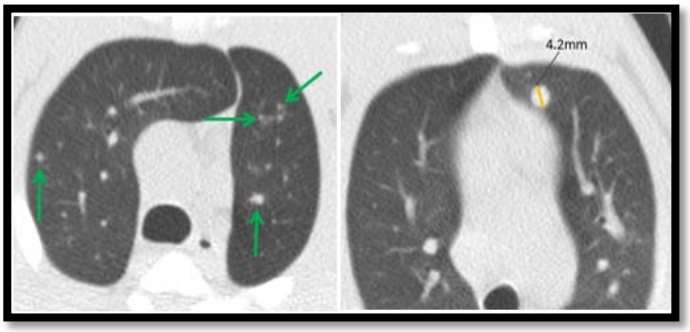

Figure 2. Isolated micronodules. Left picture shows several small isolated micronodules distributed on both upper lung lobes in an intradermic vaccinated rhesus (RIDV02) at 3rd week scan. Right picture exhibits a large isolated micronodule (4.2mm) located in the anterior bronchopulmonary segment in the left upper lobe at 3rd week scan in an intradermic vaccinated rhesus (RIDV04). Notice that nodular images not labelled correspond to pulmonary vessels.

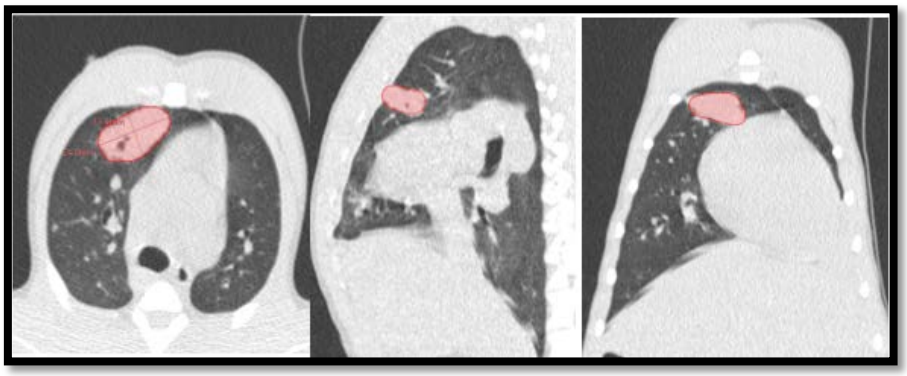

Figure 3. CT tridimensional evaluation. Example of a cavitated consolidation in an intradermic vaccinated rhesus (RIDV02) at 16th week (pictures from left to right: axial, sagittal and coronal CT scan planes). Its main axis measures 31.4mm and its volume reaches 2.308cm^3.

2.4. Experimental groups

Once CT images analysis had been concluded, we have defined five experimental groups among the thirty-five macaques, based on the genotype and their vaccination status: cynomolgus unvaccinated (CUV, n=10), cynomolgus intradermal BCG-vaccinated (CIDV, n=3), rhesus unvaccinated (RUV, n=11), rhesus aerosolized -or inhaled- BCG-vaccinated (RAEV n=6) and rhesus intradermal BCG-vaccinated (RIDV, n=5). These groups together with CT scan schedule are shown in **Suppl. Figure 1**.

2.5. Statistical assessment

To compare the mean and variance of the different observations in the two groups we used the one-way ANOVA test and Kruskal-Wallis test to determine the existence of significant differences. To compare the observed distribution of data into discrete categories, we have built a contingency table and the Fisher's test. Implementation was done in

 doi:10.20944/preprints202211.0529.v1

MATLAB and Prism. We have computed the mean with available data. In the plots we indicated with a dashed line if there was missing data. Recollected data is available in the supplementary material (**Suppl. File Raw Data**).

3. Results

3.1. Preliminary images assessment and anatomy

We were provided with high-quality CT scan images, similar to those acquired for medical diagnosis in humans. A first anatomical examination corroborated that cynomolgus macaques had smaller lung volume than rhesus macaques (**Suppl. Figure 2**). Overall, 323 consolidations were identified, 285 were found in rhesus and 38 in cynomolgus, with a median of 14 and 2 lesions per animal, respectively (**Table 1**). A total of 2228 micronodules were detected, the majority of which (1924) were found in rhesus macaques, while 304 micronodules were detected in cynomolgus (**Table 2**). Collected data revealed that lesions globally increase over time. Right lung lobes developed more consolidations in number but left lung lobes presented with a higher proportion occupied by disease. A non-significant trend was seen for the major involvement to occur in the upper lobes, which was higher in the left side (**Suppl. Figure 3**).

RUV05 presented with miliary tuberculous disease and developed hundreds of lung micronodules distributed diffusely and homogeneously (as well as extrapulmonary miliary disease). Such profuse dissemination is well known and has been described in other studies as 'widespread discrete pulmonary nodules' [63,72]. It is uncommon and denotes extremely uncontrolled infection with hematogenous dissemination. Our study was focused on pulmonary pneumonia and airway dissemination; hence, we removed the data collected from this animal from the statistical evaluation due to the different TB disease.

Table 1. Distribution of the lesions, comprising all time-points and experimental groups

EG	Consolidations			Daughter micronodules			Isolated micronodules		
	Median	Range	%	Median	Range	%	Median	Range	%
CUV (n=320)	2	[0 6]	9	5.5	[0 30]	23	5.5	[0 110]	68
CIDV (n=22)	4	[0 6]	45	0	[0 1]	5	4	[2 5]	50
C (n=342)	**2**	**[0 6]**	**11**	**3**	**[0 30]**	**22**	**4**	**[0 110]**	**67**
RUV (n=871)	12.5	[1 25]	14	36	[2 96]	49	30	[1 83]	37
RAEV (n=643)	14.5	[0 19]	12	54	[0 151]	66	18.5	[14 37]	22
RIDV (n=697)	15	[12 24]	12	55	[45 138]	53	29	[21 117]	35
R (n=2211)	**14**	**[0 25]**	**13**	**51**	**[0 151]**	**55**	**29**	**[1 117]**	**32**
TOTAL (n=2553)	**10.5**	**[0 25]**	**13**	**27.5**	**[0 151]**	**51**	**20**	**[0 117]**	**37**

EG: Experimental Group. **CUV**: unvaccinated cynomolgus; **CIDV**: intradermal BCG-vaccinated cynomolgus; **C**: total cynomolgus; **RUV**: unvaccinated rhesus; **RAEV**: aerosol BCG-vaccinated rhesus; **RIDV**: intradermal BCG-vaccinated rhesus; **R**: total rhesus

 doi:10.20944/preprints202211.0529.v1

Table 2. Distribution of micronodules, comprising all time-points and experimental groups

EG	Number (n)			Fraction
	Total	DM	IM	DM/IM
CUV	293	75	218	0.34
CIDV	12	1	11	0.09
C	**304**	**75**	**229**	**0.33**
RUV	752	428	324	1.32
RAEV	564	424	140	3.03
RIDV	611	368	243	1.51
R	**1924**	**1216**	**708**	**1.72**

DM: Daughter micronodules; **IM**: Isolated micronodules**; EG:** Experimental Group. **CUV**: unvaccinated cynomolgus; **CIDV**: intradermal BCG-vaccinated cynomolgus; **C**: total cynomolgus; **RUV**: unvaccinated rhesus; **RAEV**: aerosol BCG-vaccinated rhesus; **RIDV**: intradermal BCG-vaccinated rhesus; **R**: total rhesus.

3.2. Mtb-induced disease is worse in rhesus macaques.

In order to exemplify the complexity of the operational procedure, **Figure 4** illustrates a particular evolution in one case (RIDV02). Overall development of the natural infection in control groups is summarized in **Figure 5**. The temporal evolution of the lesions is shown per animal, based on the size and localization per lobe in a 2D representation. Each pair of lungs is reshaped according to each individual volume (adapted to the image obtained from macaque RUV04).

At first sight this summary highlights the greater severity of the infection in rhesus macaques. In particular, at week 3 cynomolgus macaques developed a low number of lesions, with a small volume, which were usually well controlled and exhibited minimal enlargement with time. Lesions were not identified in one individual (CUV10) although infection was confirmed by other methodologies. Other individuals showed a decline in condition only at the late phase (15th week) of the study, e.g., CUV07, in which an extraordinary growth of consolidations was detected on CT images, that was probably due to total main bronchus stenosis (despite it is uncommon in cynomolgus).

In contrast, lesions in rhesus were abundant and larger at week 3, usually exhibiting enlargement and dissemination over time. Poor control leading to extreme disease was evident in RUV05 (which developed profuse miliary dissemination, described above) and also in RUV06, RUV08; these animals had to be euthanized before finishing the monitor period due progressive disease that met humane endpoint criteria. However, there was at least one case in a rhesus where a spontaneous weak regression of lesions was observed (RUV10) (**Figure 5**).

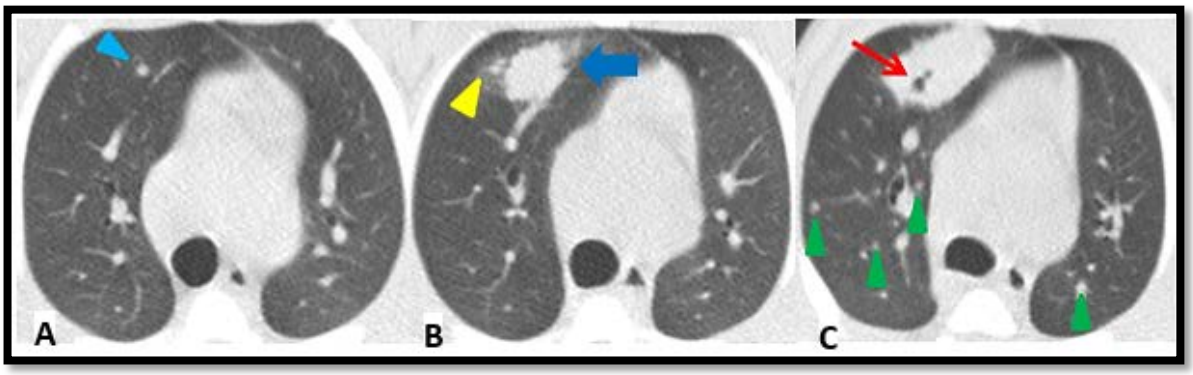

Figure 4. Pulmonary tuberculosis progression. Lesions from 3rd to 16th post-challenge week in an intradermic vaccinated rhesus (RIDV02). **Picture A**: a 3rd week CT shows a lesion in the anterior bronchopulmonary segment in the right upper lobe that initially is a 2.1mm isolated micronodule (light blue arrowhead). **Picture B**: an 11th week scan exhibits its progression to a consolidation (dark blue arrow) and the development of two daughter micronodules (yellow arrowhead). **Picture C**: CT performed at 16th week shows a higher enlargement of the consolidation, in which has arisen a cavitation (red arrow). Moreover, some small isolated micronodules (green arrowheads) have appeared distributed on both lungs. Notice that nodular images not labelled correspond to pulmonary vessels.

Preprints (www.preprints.org) | NOT PEER-REVIEWED | Posted: 29 November 2022 doi:10.20944/preprints202211.0529.v1

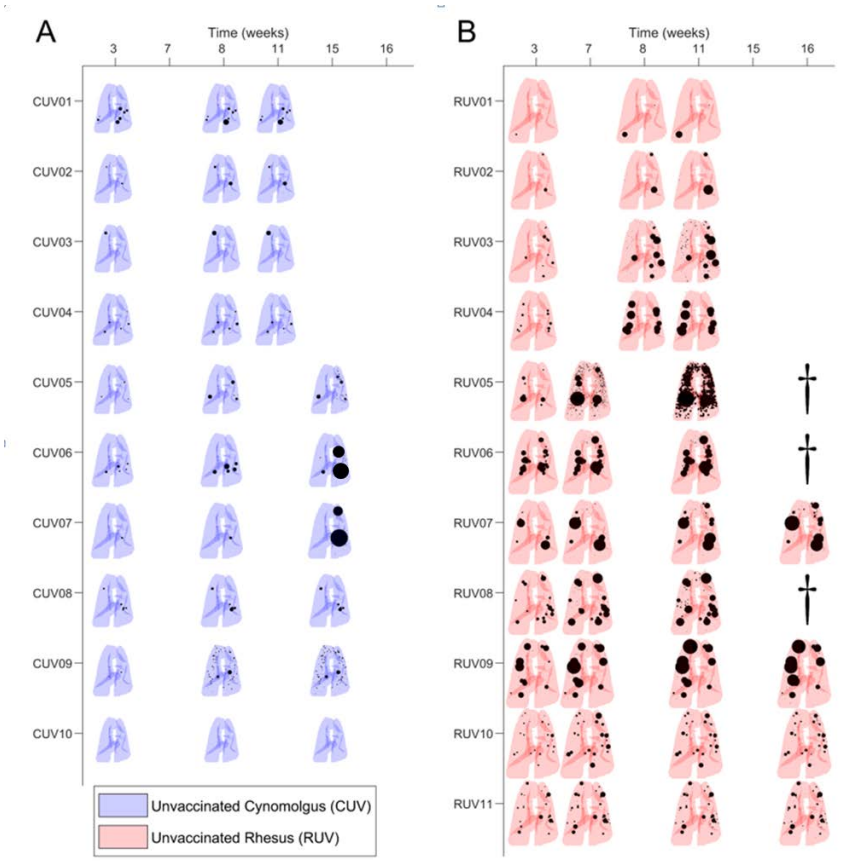

Figure 5. Evolution of lesions in unvaccinated macaques. The size and location of tuberculosis lesions determined from computed tomography (CT) scan taken at specific times after initial infection are shown in each pair of lungs. Lesions (consolidations and micronodules), in black, are represented as spheres of the measured volume and located in the segment where they are identified. **Picture A**, in blue, reconstructions of CT scans from each unvaccinated cynomolgus. **Picture B**, in red, reconstructions of CT scan collected from each unvaccinated rhesus. Macaques RUV05, RUV06 and RUV08 marked with dagger symbol were euthanized before the end of the study.

Cynomolgus macaques developed significantly fewer lung consolidations and micronodules, resulting in a smaller pulmonary volume occupation than that seen in rhesus macaques, as shown in **Table 1** and **Figure 6**. Cynomolgus macaques also had a significantly lower percentage of daughter micronodules than rhesus macaques (**Tables 1** and **2,** and **Figure 7**). The overall ratio of daughter/isolated micronodules for non-vaccinated macaques comprising all time points is 1.32 and 0.34 for rhesus and cynomolgus, respectively. Similarly, the number of consolidated lesions with daughter micronodules associated was also significantly lower in cynomolgus macaques (**Table 3**). These data reflect a higher containment of lesions' progression in cynomolgus.

Preprints (www.preprints.org) | NOT PEER-REVIEWED | Posted: 29 November 2022 doi:10.20944/preprints202211.0529.v1

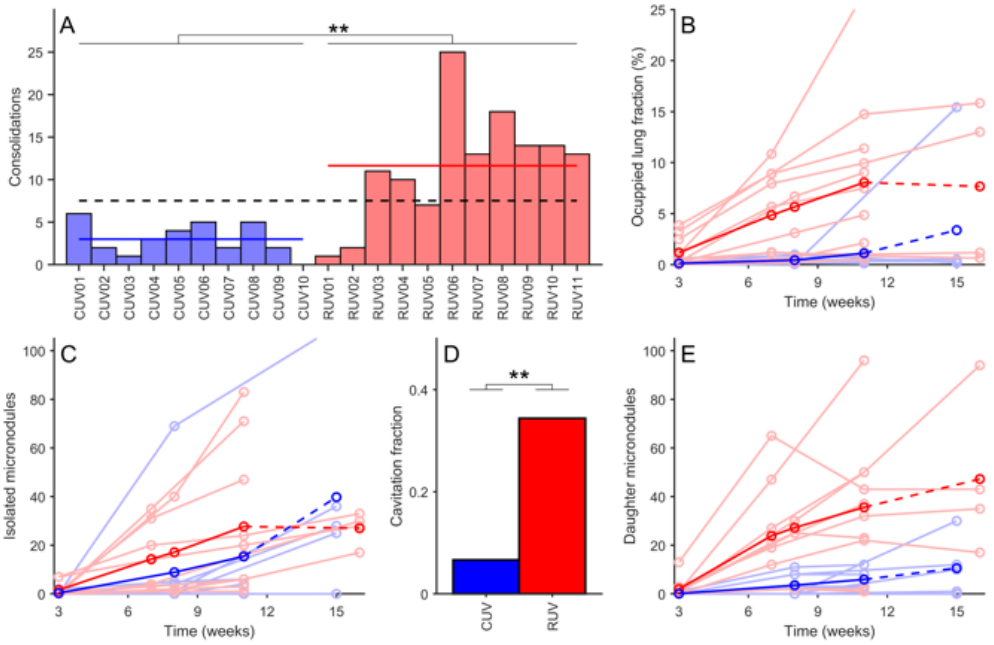

Figure 6. Analysis of unvaccinated macaques. Picture A Displays the number of identified consolidations for each macaque at the end of the study. In light blue, each non-vaccinated cynomolgus (CUV) macaque is represented. In blue, the mean number of lesions for CUV macaques. In light red, each non-vaccinated rhesus (RUV) macaque is represented. In red, the mean number for RUV macaques. Dotted black line shows the mean value for all non-vaccinated macaques. **Picture B** shows the occupied lung fraction for each macaque. **Picture C** shows the number of isolated micronodules for each macaque. **Picture D** shows the fraction of consolidations that present cavitation in any CT scan. **Picture E** shows the number of daughter micronodules for each macaque. In **Pictures B, C and E** each circle represents an experimental measurement from computed tomography (CT) scans. Light lines represent the evolution for each macaque. Darker lines are the mean lines value. Dotted lines are used when one or more macaques are not considered because they were euthanized, or the study ended before that time point. Data is analyzed through One way ANOVA test (** $p < 0.01$).

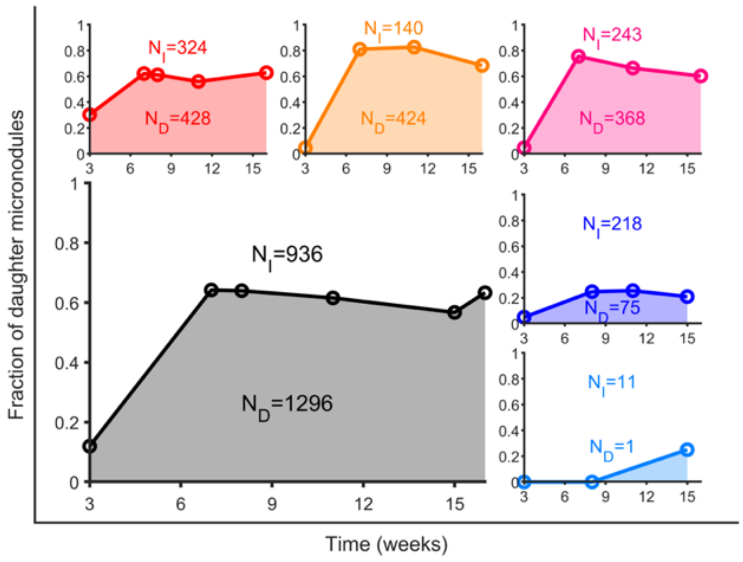

Figure 7. Fraction of daughter micronodules. Number of total isolated micronodules (N_I) and number of total daughter micronodules (N_D) are shown in grey. Total number of micronodules is computed considering all CT scans independently. Total fractions are depicted in blue for unvaccinated cynomolgus (CUV); in cyan, for intradermal vaccinated cynomolgus (CIDV); in red, for unvaccinated rhesus (RUV); in orange, for aerosol vaccinated rhesus (RAEV); and in purple, for intradermal vaccinated rhesus (RIDV).

Preprints (www.preprints.org) | NOT PEER-REVIEWED | Posted: 29 November 2022 doi:10.20944/preprints202211.0529.v1

Table 3. Distribution of consolidations with daughter micronodules, comprising all time-points and experimental groups

EG	Consolidations with DM				DM per consolidation	
	n	%	Median	Range	Median	Range
CUV (n=29)	19	66	2	[0 4]	3	[1 15]
CIDV (n=10)	1	10	0	[0 1]	1	[1 1]
C (n=39)	**20**	**51**	**1**	**[0 4]**	**3**	**[1 15]**
RUV (n=121)	111	92	11.5	[1 24]	3	[1 15]
RAEV (n=80)	79	99	14.5	[0 19]	3.5	[1 15]
RIDV (n=88)	84	95	14	[11 24]	3	[1 15]
R (n=289)	**274**	**95**	**14**	**[0 24]**	**3**	**[1 15]**
Total (n=328)	**294**	**90**	**9**	**[0 24]**	**3**	**[1 15]**

DM: Daughter micronodules. **EG:** Experimental Group. **CUV**: unvaccinated cynomolgus; **CIDV**: intradermal BCG-vaccinated cynomolgus; **C**: total cynomolgus; **RUV**: unvaccinated rhesus; **RAEV**: aerosol BCG-vaccinated rhesus; **RIDV**: intradermal BCG-vaccinated rhesus; **R**: total Rhesus.

The size of consolidated lesions was highly dependent on the number of daughter micronodules. This is reflected in the **Figure 8** where a clear and significant correlation is noted between the size of the consolidated lesions and the number of daughter micronodules, regardless of the vaccination status. This positive slope is markedly higher in rhesus macaques. In addition, a greater portion of occupied pulmonary volume is correlated to a higher number of isolated micronodules (**Suppl. Figure 4**), so the higher infectious involvement of lungs, the higher rate of pulmonary dissemination (local and endobronchial reinfections, which fits with the Dynamic Hypothesis [52]).

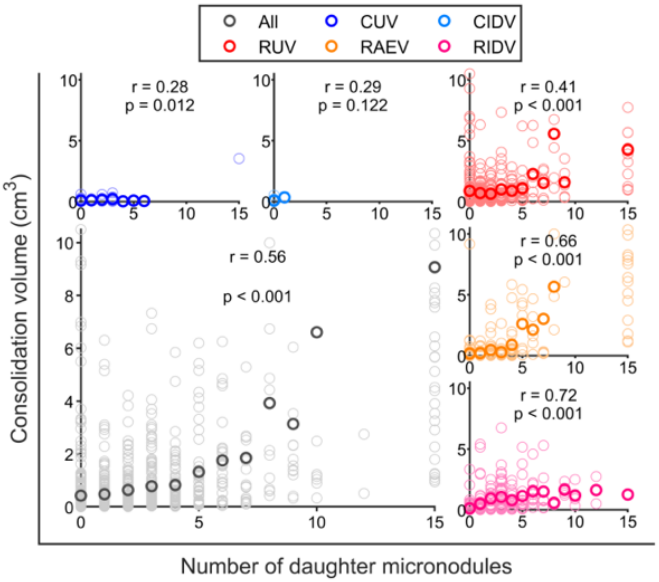

Figure 8. Correlation between the volume of consolidated lesions and the number of daughter micronodules. Light circles represent a single consolidation. Dark circles represent the mean volume value of all consolidations that present the same number of daughter micronodules. Correlation value between both quantities is written as *r*. The significance of correlation value is determined from the *p-value,* that is shown under correlation value, according to the X test. In blue, unvaccinated cynomolgus (CUV); in cyan, intradermal vaccinated cynomolgus (CIDV); in red, unvaccinated rhesus (RUV); in orange, aerosol vaccinated rhesus (RAEV); in purple, intradermal vaccinated rhesus (RIDV); in grey, all macaques (all).

Preprints (www.preprints.org) | NOT PEER-REVIEWED | Posted: 29 November 2022 doi:10.20944/preprints202211.0529.v1

We also detected some transitional lesions, which correspond to isolated micronodules that increased to a size of more than 4.4mm from one CT to the next, thus becoming a consolidation (**Suppl. Table 1**). This enlargement occurred mainly in the early phase between the third and eighth-week post-challenge. Remarkably, rhesus developed directly a large number of consolidations in the early phase after infection, in contrast to cynomolgus; hence, transitional lesions represent a higher impact on cynomolgus. Importantly, there is no significant difference between both macaque genotypes considering the progression of isolated micronodules towards consolidated lesions.

3.3. BCG vaccination in rhesus macaques reduces the number of lesions, although intradermal vaccination better controls daughter micronodules

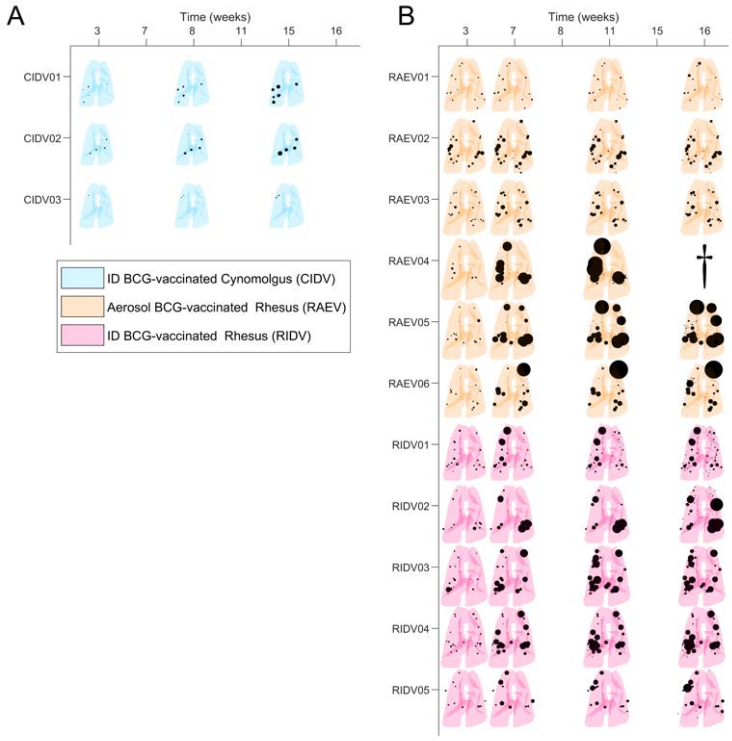

Figure 9. Lesions evolution in vaccinated macaques. Each pair of lungs show the size and location of tuberculosis lesions determined from computed tomography (CT) scan taken after initial infection. Lesions (consolidations and micronodules), in black, are represented as spheres of the measured volume and located in the segment where they were identified. **Picture A,** in cyan, the reconstructions of lungs from intradermal vaccinated cynomolgus (CIDV) for each CT scan. **Picture B,** in orange, the reconstructions of lungs from aerosol vaccinated rhesus (RAEV) for each CT scan. In purple, the reconstructions of lungs from intradermal vaccinated rhesus (RIDV) for each CT scan. Macaque RAEV04 marked with dagger symbol was euthanized before the planned end of study.

Initial evaluation of the impact of vaccination in macaques suggested that a protective effect appeared by the 3rd week post-challenge (**Figures 5,7** and 9). But a deeper analysis revealed that protection measured in terms of infected (i.e., occupied lung fraction at week 3), did not appear to provide a reliable indicator of later outcome (**Suppl. Figures 5** and **6**). When each disease volume fraction was normalized against the maximum infiltrated lung volume per macaque (**Figure 10**) it revealed a clear impact of the vaccination in cynomolgus macaques early after challenge, although it does not last until the end of the monitoring time.

Preprints (www.preprints.org) | NOT PEER-REVIEWED | Posted: 29 November 2022 doi:10.20944/preprints202211.0529.v1

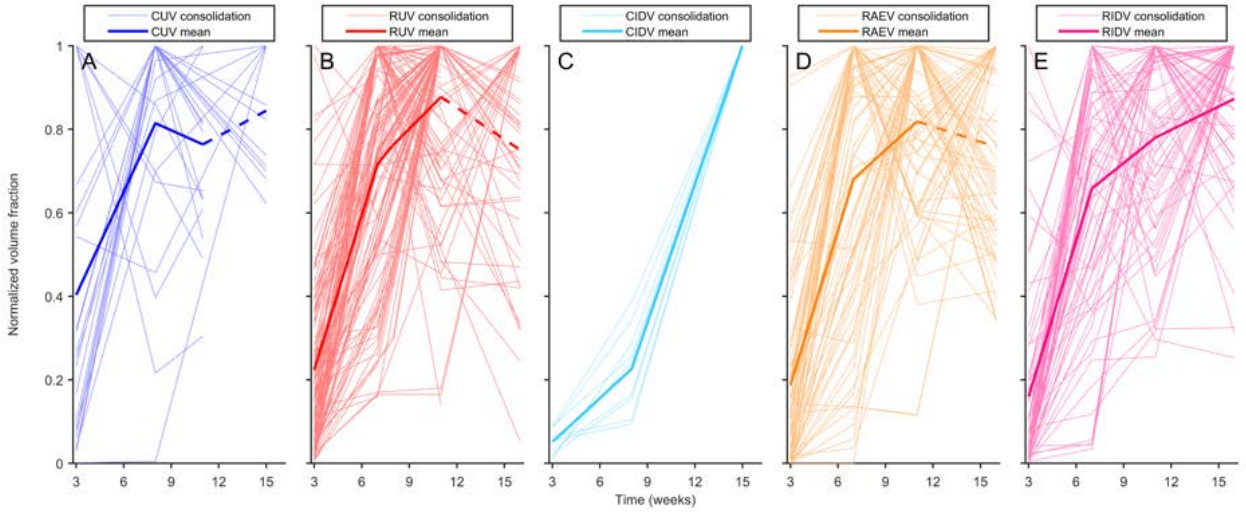

Figure 10. Evolution of normalized occupied lung volume per each individual and experimental group. Volume of each involved area is divided by the maximum occupied lung volume reached by each individual. **Picture A** light blue lines indicate values for unvaccinated cynomolgus (CUV). Blue line indicates the mean value of all light blue lines. **Picture B** shows light red lines for unvaccinated rhesus (RUV). Red line is the mean value of all light red lines. **Picture C** shows light cyan lines for intradermal vaccinated cynomolgus (CIDV). Cyan line shows the mean value of all light blue lines. **Picture D** shows light orange lines are for aerosol vaccinated rhesus (RAEV). Orange line is the mean value of all light blue lines. **Picture E** shows light purple lines are for intradermal vaccinated rhesus (RIDV). Purple line is the mean value of all light blue lines. Dotted line appears when some lesions where data are not available due to study finalization or euthanized macaque.

Due to the correlation between the volume of the consolidated lesions and the number of daughter micronodules, we investigated if vaccination had an impact on this fraction of micronodules in relation to the enlargement of consolidated lesions. And this was the case. Looking at **Figure 7**, vaccination clearly reduced this fraction in all vaccinated macaques, although temporally in rhesus, as it rapidly resumed by week 7 to 8. The reduction of this parameter only prevails in cynomolgus until 15th week.

Evaluation of the route of vaccination in rhesus macaques revealed an interesting paradox. Whilst aerosol vaccination (RAEV) reduced the total number of micronodules, more than intradermal vaccination (RIDV), a significantly greater fraction of daughter micronodules were present (3.03) (**Table 4**). Thus, the protective effect of RAEV relies on the reduction of the total number of micronodules (**Tables 2** and **3**) rather than control of subsequent consolidation development. Even though the reduction of total micronodules was weaker in the RIDV, its effect was noted in both types of micronodules. Even when this fraction is slightly higher in RIDV (1.51) than non-vaccinated (RUV) (1.32) (**Table 2**). At the end this means that progression towards consolidation in a hypothetical later time-point would be faster in the RAEV group, followed by RIDV and RUV.

The effect of vaccination in rhesus was also observed as a decrease in the proportion of consolidated lesions that were associated with daughter micronodules, which was more pronounced and significant after intradermal (95%) than after aerosol vaccination (99%) (**Tables 3** and **5**). This effect is even more pronounced in cynomolgus macaques, although in this case there is no variation in the proportion of isolated and daughter micronodules between vaccinated (intradermal) and unvaccinated groups (**Tables 2** and **4**). This can be explained because, as indicated above, cynomolgus are able to spontaneously stop the progression of the consolidated lesions soon after the infection (i.e., before week 3rd after challenge).

Preprints (www.preprints.org) | NOT PEER-REVIEWED | Posted: 29 November 2022 doi:10.20944/preprints202211.0529.v1

Table 4. Differences in the proportion of daughter and isolated micronodules per experimental group.

Contingency table. Numbers correspond to p values (Fisher's test)

EG	CUV	CIDV	C	RUV	RAEV	RIDV	R
CUV	ND						
CIDV	0,3057	ND					
C	ND	ND	ND				
RUV	ND	ND	ND	ND			
RAEV	ND	ND	ND	<0,0001	ND		
RIDV	ND	ND	ND	0,2431	<0,0001	ND	
R	ND	ND	<0,0001	ND	ND	ND	ND

EG: Experimental Group. **CUV:** unvaccinated cynomolgus; **CIDV:** intradermal BCG-vaccinated cynomolgus; **C:** total cynomolgus; **RUV:** unvaccinated rhesus; **RAEV:** aerosol BCG-vaccinated rhesus; **RIDV:** intradermal BCG-vaccinated rhesus; **R:** total Rhesus.

Table 5. Differences on the proportion of consolidated lesions associated to daughter micronodules per experimental group.

Contingency table. Numbers correspond to p values (Fisher's test)

EG	CUV	CIDV	C	RUV	RAEV	RIDV	R
CUV	ND						
CIDV	0,0014	ND					
C	ND	ND	ND				
RUV	ND	ND	ND	ND			
RAEV	ND	ND	ND	0,0585	ND		
RIDV	ND	ND	ND	0,0355	>0,999	ND	
R	ND	ND	<0,0001	ND	ND	ND	ND

EG: Experimental Group. **CUV:** unvaccinated cynomolgus; **CIDV:** intradermal BCG-vaccinated cynomolgus; **C:** total cynomolgus; **RUV:** unvaccinated rhesus; **RAEV:** aerosol BCG-vaccinated rhesus; **RIDV:** intradermal BCG-vaccinated rhesus; **R:** total Rhesus.

 doi:10.20944/preprints202211.0529.v1

3.4. Cavitation is more probable in larger lesions and contact with pleura appear to impact on tuberculosis progression

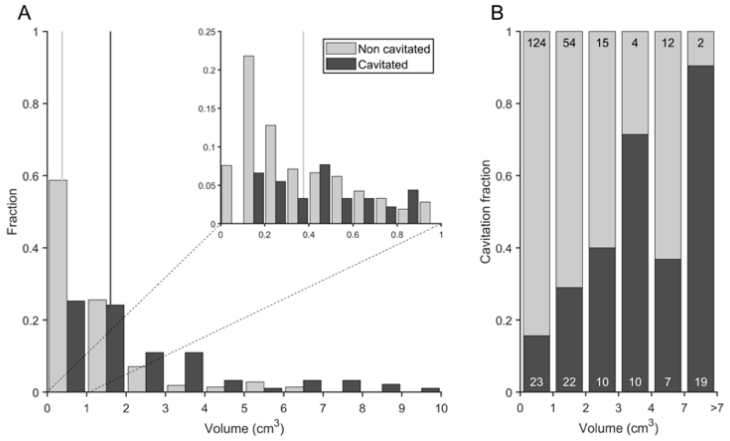

Figure 11. Relation between the fraction and the volume of cavitated consolidations in rhesus macaques. **A** Consolidation volume distribution for non cavitated (light grey) and cavitated (dark grey) lesions. Vertical lines show the median values for each of the subsets. **B** Cavitation fraction for the consolidations that are in a desired range of volumes: 0 to 1 cm^3, 1 to 2 cm^3, 3 to 4 cm^3, 4 to 7 cm^3 and consolidations bigger than 7 cm^3. The number of non-cavitated consolidations observed is shown in black, at the top. In white, at the bottom, the number of cavitated consolidations observed.

Cavitation occurred mostly in rhesus and especially at late phase, where 34.4% of consolidated lesions developed cavities in nonvaccinated rhesus (RUV), closely followed by 28.4% of the aerosolized (RAEV) and by 24.3% of the ID (RIDV). Analysis of cavitation in rhesus (**Figure 11**) revealed a relationship with lesion size (p<0,0001): the higher the consolidation volume, the higher rate of cavitation, with cavitation more probable in lesions greater than 2 cm^3, which represents a rate of 57%. In contrast, almost 80% of lesions from 0 to 2 cm^3 did not cavitate. The anatomic distribution of lesions was not found to influence cavity formation.

We also evaluated the relationship between consolidations and pleura, in order to investigate if the contact with pleura favoured the encapsulation process of the lesions and stopped enlargement. As shown in **Suppl. Figures 7**, the group of smaller lesions (up to 0.5 cm^3, which accounts for the higher number of consolidations) were mainly not in contact with the pleura, especially in rhesus (which have bigger lungs), and from this size on, consolidations were mainly in contact with the pleura.

The next step was to determine if consolidations changed between two consecutive CT scans, with respect to their size and distance from pleura. So, we evaluated the change in the volume together with the relationship with the contact with pleura. We have explored the change of the relative volume gradient, explained through a boxplot (**Figure 12**). In this regard, differences are significant (p=0,04 Kruskal-Wallis) in cynomolgus for those consolidations which make contact with the pleura, as they remain stable in volume. Thus, pleural contact is protective in cynomolgus, preventing the progression of consolidations, and this trend is irrespectively of their vaccination status. In contrast, in rhesus, consolidations that enlarge and make contact with pleura do not experience a volume control, because the increase in the size is too fast and large to benefit from the encapsulation process activated by the pleura.

Preprints (www.preprints.org) | NOT PEER-REVIEWED | Posted: 29 November 2022 doi:10.20944/preprints202211.0529.v1

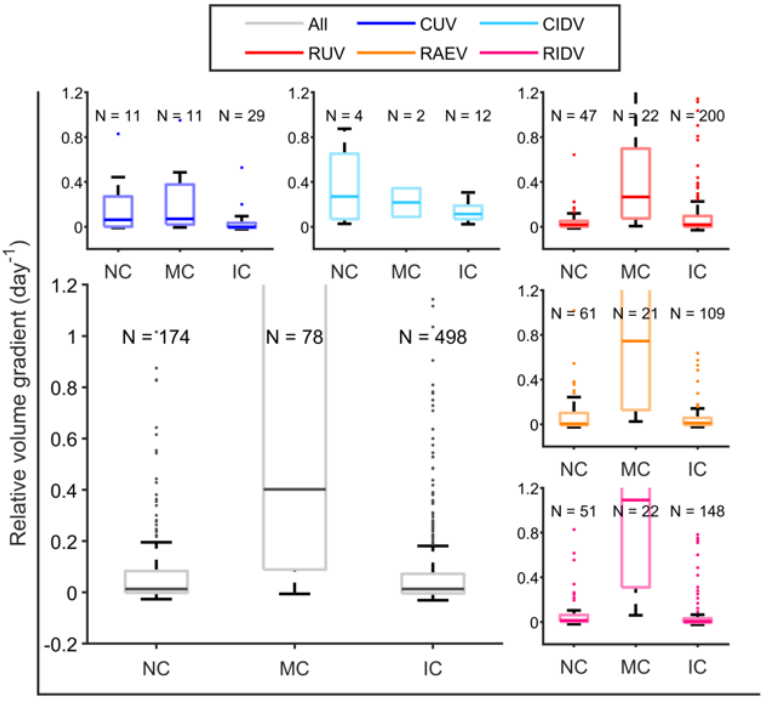

Figure 12. Volume increase of the consolidations in relation with the contract with pleura. The increase of volume is expressed as relative gradient per day between two consecutive CT scans. Consolidations are classified between: not in contact (NC), if in both CT scans it is not in contact with pleura; make contact (MC), if it is not in contact in the first CT but it is in contact in the second; and in contact (IC), if in both CT scans it is in contact with pleura. It is indicated how many cases are identified for each classification. In blue, unvaccinated cynomolgus (CUV); in cyan, intradermal vaccinated cynomolgus (CIDV); in red, unvaccinated rhesus (RUV); in orange, aerosol vaccinated rhesus (RAEV); in purple, intradermal vaccinated rhesus (RIDV); in grey, all macaques (all).

4. Discussion

Tuberculosis remains a major killer of humankind, and the lack of a surrogate of protection, means there is a constant need for the field to find experimental models able to elucidate new biomarkers and correlates to assist the development of new more effective vaccines. Nowadays, the macaque is considered the most clinically relevant experimental infection model of tuberculosis given its physiological closeness with humans and the similarity in disease manifestations. However, the macaque does lack the interlobular septa, present in human lungs, which have been demonstrated to provide a protective mechanism in the minipig model [9]. The outcome of experimental infection with *Mycobacterium tuberculosis* has been widely studied in macaques, and models established in rhesus and cynomolgus have been used to assess the efficacy of new drugs and vaccines. Mtb infection in cynomolgus macaques resembles what occurs in humans, with the display of the whole spectrum of human TB, mainly controlling the infection and becoming latently infected. In contrast, rhesus macaques experience a rapid dissemination of the infection in the lung, with the development of active TB in almost all the infected animals, a characteristic that enables the capacity of vaccines to protect against this progression to be assessed using manageable group sizes [73].

There is little data on vaccines showing significant protection against Mtb challenge in the macaque model with reports limited to BCG delivered intravenously (IV) for which the clinical deplorability of which is debatable, or a CMV-vectored vaccine [74] which is at pre-clinical stage of development, and MTBVAC [28]. Whilst there is very little data on immune responses induced in NHP and human after exactly the same immunizations, the immune profiles induced following immunization with MTBVAC were shown to reflect those identified in human clinical trials [75–77]. This concordance between immune profiles measured in clinical trials and a macaque pre-clinical assessment of a novel TB vaccine candidate, demonstrating significantly improved outcome after Mtb challenge, is a promising indication that the protection provided by MTBVAC vaccination to macaques will translate to the human population.

The ability to demonstrate vaccine efficacy is critical, and the role of the macaque models in vaccine development is

 doi:10.20944/preprints202211.0529.v1

underpinned by the ability to measure vaccine-associated impacts on the disease that develops following infectious challenge.

Our approach has been to test a new way to interpret data derived from these models based on the 'Bubble Model', that defines the progression from latent to active TB supported by the interpretation of disease progression defined in the studies on the C3HeB/FeJ mice [49,54,78,79]. Like humans, the C3HeB/FeJ mouse model establishes that the development of a large lesion after the Mtb infection requires a strong inflammatory response in the initial lesions, the induction of daughter micronodules around them and the coalescence of all lesions.

To evaluate this concept in macaques, we have used CT images obtained previously from studies using an experimental model of low dose aerosol exposure, thus closely resembling what is thought to happen in the natural infectious process, where CT scans were collected at several time points to monitor the evolution of the infection in each animal [13,14,28]. In line with previous reports, three weeks after infection more large lesions were identified in rhesus macaques compare to cynomolgus macaques, which has been related with the development of a stronger inflammatory response in the former [14,40]. These lead to an exudative lesion, a hallmark of progression towards active TB [51] and a key issue for its development, according to the Bubble Model.

So far, the assessment of new vaccines has been mainly based on the induction of an immune response and a reduction in disease burden measured using pathology scoring, that included a semiquantitative approach of the involvement of lungs and other organs, as well as imaging based measures through PET-CT [11,45], CT evaluation [28,80], histology based measures (e.g. granuloma staging and prevalence), together with bacterial burden in organs and changes in clinical parameters.

There is quite experience in using imaging as a tool to evaluate BCG efficacy in animal models, with special interest in NPH. However, some studies have appeared during the last few years, which are mainly focused on BCG alternative routes. White *et al.* (2020) [28] analysed CT images in rhesus macaques and used a quantitative score system for the estimation of TB-induced disease burden [63]; Sharpe *et al.* (2016) [81] and recently Sibley *et al.* (2021) [29] used MRI images in ex-vivo lungs from macaques to determine pulmonary disease burden applying stereology [46], as well as counting of discrete and coalescent lesions; Darrah *et al.* (2020) [72] and DiFazio *et al*. (2016) [82] performed PET-TC images in macaques and mainly evaluated grade of tuberculous activity by measuring global lung parenchyma FDG avidity, as well as counting lesions (which were called granulomas). Moreover, there are some experiences including other animal models, as Kraft et al. (2004) [83] analysed ex-vivo lungs from guinea pigs using MRI, and described their imaging appearance, their anatomical distribution and nodules counting.

Previous analysis of these images highlighted the early reduction of micronodules after BGC vaccination [28]. Our work has been able to advance deeper in the exploitation of this data by differentiating the nodules related with the consolidated lesions, daughter micronodules from the isolated ones. According to the 'Bubble model', daughter micronodules emerge from an initial isolated micronodules, increase in size, consolidate creating larger nodules, which in turn develops more daughter micronodules, a process that enlarges the lesion to the point that it becomes visible by chest X ray, the hallmark to classify an Mtb infection as active TB [51]. Data from the C3HeB/FeJ model suggests this progression mainly develops at the beginning of the infection, when there is still a lower impact of the adaptive immune response. This is characterized by the infiltration of neutrophiles, that allows the extracellular growth of Mtb, fuelling enlargement and allowing the spread of close new infectious foci due to the drainage of infected foamy macrophages, which in turn attracts new neutrophils, causing the development of daughter lesions [54]. This led us to draw a parallel with the NHP model. On one hand rhesus develop a highly inflammatory lesions with a high neutrophilic infiltration, a process that might be related with the progression associated to the development of daughter micronodules. On the contrary, cynomolgus develop less inflammatory and more contained lesions [40] which would link to a reduced capacity to generate daughter micronodules. The lower inflammatory response and thus, the lower capacity to generate daughter cells, allows the fibroblasts to encapsulate the lesion stopping its progression [9] and explains why the vicinity of the pleura, and its encapsulation capacity, has only a protective effect in cynomolgus.

Our data provides two new measures of pulmonary disease burden induced following infection with *M. tuberculosis* namely, the ratio daughter/isolated micronodules and the percentage of consolidated lesions linked to daughter micronodules identified through CT in macaques. These measures provide a new tool to evaluate the protective effect of the licenced vaccine (BCG) and revealed differences in disease progression following either intradermal or mucosal (inhaled) administration, even when both routes where not able to reduce the number of consolidated lesions and generated a similar reduction in the number of micronodules. Whilst this mucosal aerosol vaccination was better able to

reduce the number of isolated micronodules, potentially because of a better capacity to reach and stimulate the immune response in the whole lung, intradermal administration should an improved ability to reduce the emergence of daughter micronodules, which are the ones responsible for the progression towards active TB.

In summary, we have defined a new tool for the evaluation of pulmonary disease induced by Mtb infection, through the description of 'daughter micronodules', which provides a better understanding of the progression of TB and which can be applied for testing new vaccines. This is also amenable for development as a machine learning tool, as nodules are easily identifiable in CT images and can be quantified. Enhanced measures of TB disease burden and progression, such as those reported here will refine the models used in the development of new vaccines and reduce the number of animals required, consequently providing important scientific and welfare benefits.

Supplementary Materials: The following supporting information can be downloaded at: www.mdpi.com/xxx/s1. Figure S1: Experimental groups and CT scan acquisition schedule; Figure S2: Lung size in macaques; Figure S3: Occupied volume fraction per lung lobe; Figure S4: Correlation between the occupied lung fraction and the number of isolated micronodules; Table S1: Summary lesions found; Figure S5: Cynomolgus vaccine effect analysis; Figure S6: Rhesus vaccine effect analysis; Figure S7: Volume distribution of consolidations in contact and not in contact with pleura.

Author Contributions: Conceptualization, I.N., M.C., P.-J.C and C.V; methodology, P.J.C, C.P., J.B, I.N., M.C and C.V.; software, J.B.; validation, S.A.S, A.D.W, J.B., C.V. and P.J.C.; formal analysis, C.P.; investigation, I.M, M.C and P.J.C.; resources, S.A.S and A.D.W.; data curation, C.P and M.C.; writing—original draft preparation I.N and M.C.; writing—review and editing, P.J.C and S.A.S.; visualization, J.B.; supervision, P.J.C and C.P.; project administration, C.V., P.J.C. and J.B. All authors have read and agreed to the published version of the manuscript.

Funding: This research was funded by "La Caixa" Foundation (ID 100010434), under agreement LCF/PR/GN16/10290002.

Institutional Review Board Statement: The study design and all procedures were approved by the Public Health England, Porton Down Animal Welfare and Ethical Review Body, and authorised under an appropriate UK Home project license.

Informed Consent Statement: "Not applicable."

Data Availability Statement: Raw data will be available as supplementary data.

Acknowledgments: We thank to colleges in Unitat de Tuberculosi Experimental for their support, as well as to Ignasi Guasch and colleges from the Thorax Radiology Department in Hospital Universitary Germans Trias Pujol

Conflicts of Interest: The authors declare no conflict of interest.

References

1. World Health Organization. *Global Tuberculosis Report 2021*; WHO: Geneva, Switzerland, 2021.
2. World Health Organization. Impact of the COVID-19 pandemic on TB detection and mortality in 2020. **2021**; WHO: Geneva, Switzerland, 2021
3. Pai, M; Kasaeva, T; Swaninathan, S. COVID-19's devastating effect on tuberculosis care — A path to recovery. *N Engl J Med.* **2022**, *386*, 1490-1493.
4. World Health Organization. End TB Strategy. **2015**; WHO: Geneva, Switzerland, 2021
5. Cardona, P.J. What we have learned and what we have missed in tuberculosis pathophysiology for a new vaccine design: searching for the "Pink Swan." *Front. Immunol.* **2017**, *8*, 556.
6. Wallis, R.S.; Maeurer, M.; Mwaba, P.; Chakaya, J.; Rustomjee, R.; Migliori, G.B.; Marais, B.; Schito, M.; Churchyard, G.; Swaminathan, S.; et al. Tuberculosis-advances in development of new drugs, treatment regimens, host-directed therapies, and biomarkers. *Lancet Infect Dis* **2016**, *16*, e34–e46.
7. Urbanowski, M.E.; Ordonez, A.A.; Ruiz-Bedoya, C.A.; Jain, S.K.; Bishai, W.R. Cavitary tuberculosis: the gateway of disease transmission. *Lancet Infect Dis* **2020**, *20*, e117–e128.
8. Ihms, E.A.; Urbanowski, M.E.; Bishai, W.R. Diverse cavity types and evidence that mechanical action on the necrotic granuloma drives tuberculous cavitation. *Am. J. Pathol.* **2018**, *188*, 1666–1675.
9. Gil, O.; Díaz, I.; Vilaplana, C.; Tapia, G.; Díaz, J.; Fort, M.; Cáceres, N.; Pinto, S.; Caylà, J.; Corner, L.; et al. Granuloma encapsulation is a key factor for containing tuberculosis infection in minipigs. *PLoS One* **2010**, *5*, e10030.
10. Wong, E.A.; Joslyn, L.; Grant, N.L.; Klein, E.; Lin, P.L.; Kirschner, D.E.; Flynn, J.A.L. Low levels of T cell exhaustion in tuberculous lung granulomas. *Infect Immun* **2018**, *86*, e00426-18.
11. Lin, P.L.; Coleman, T.; Carney, J.P.J.; Lopresti, B.J.; Tomko, J.; Fillmore, D.; Dartois, V.; Scanga, C.; Frye, L.J.; Janssen, C.; et al. Radiologic responses in cynomolgus macaques for assessing tuberculosis chemotherapy regimens. *Antimicrob Agents Chemother.* **2013**, *57*, 4237–4244.
12. Ramakrishnan, L. Revisiting the role of the granuloma in tuberculosis. *Nat Rev Immunol.* **2012**, *12*, 352–366.
13. White, A.D.; Sibley, L.; Gullick, J.; Sarfas, C.; Clark, S.; Fagrouch, Z.; Verschoor, E.; Salguero, F.J.; Dennis, M.; Sharpe, S. TB and SIV coinfection; a model for evaluating vaccine strategies against TB reactivation in asian origin cynomolgus macaques: a pilot study using BCG vaccination. *Vaccines* **2021**, *9*, 1–14.
14. Sharpe, S.; White, A.; Gleeson, F.; McIntyre, A.; Smyth, D.; Clark, S.; Sarfas, C.; Laddy, D.; Rayner, E.; Hall, G.; et al. Ultra-low dose aerosol challenge with *Mycobacterium tuberculosis* leads to divergent outcomes in rhesus and cynomolgus macaques. *Tuberculosis* **2016**, *96*, 1–12.
15. Lin, P.L.; Rodgers, M.; Smith, L.; Bigbee, M.; Myers, A.; Bigbee, C.; Chiosea, I.; Capuano, S. V.; Fuhrman, C.; Klein, E.; et al. Quantitative comparison of active and latent tuberculosis in the cynomolgus macaque model. *Infect Immun* **2009**, *77*, 4631–4642.
16. Lin, P.L.; Flynn, J.L. The end of the binary era: revisiting the spectrum of tuberculosis. *J Immunol.* **2018**, *201*, 2541–2548.
17. Zwerling, A.; Behr, M.A.; Verma, A.; Brewer, T.F.; Menzies, D.; Pai, M. The BCG world atlas: a database of global BCG vaccination policies and practices. *PLoS Med.* **2011**, *8*, e1001012.
18. Lancione, S.; Alvarez, J.V.; Alsdurf, H.; Pai, M.; Zwerling, A.A. Tracking changes in national BCG vaccination policies and practices using the BCG world atlas. *BMJ Glob Heal.* **2022**, *7*, e007462.
19. Abubakar, I.; Pimpin, L.; Ariti, C.; Beynon, R.; Mangtani, P.; Sterne, J.; Fine, P.; Smith, P.; Lipman, M.; Elliman, D.; et al. Systematic review and meta-analysis of the current evidence on the duration of protection by bacillus Calmette-Guérin vaccination against tuberculosis. *Health Technol Assess.* **2013**, *17*, 1-372.
20. Rodrigues, L.C.; Diwan, V.K.; Wheeler, J.G. Protective effect of BCG against tuberculous meningitis and miliary tuberculosis:

a meta-analysis. *Int J Epidemiol.* **1993**, *22*, 1154-8.

21. Dockrell, H.M.; Smith, S.G. What have we learnt about BCG vaccination in the last 20 years? *Front Immunol.* **2017**, *13*, 1134
22. Trunz, B.B.; Fine, P.; Dye, C. Effect of BCG vaccination on childhood tuberculous meningitis and miliary tuberculosis worldwide: a meta-analysis and assessment of cost-effectiveness. *Lancet* **2006**, *367*, 1173–1180.
23. Colditz, G.A.; Brewer, T.F.; Berkey, C.S.; Wilson, M.E.; Burdick, E.; Fineberg, H. V.; Mosteller, F. Efficacy of BCG vaccine in the prevention of tuberculosis: meta-analysis of the published literature. *JAMA* **1994**, *271*, 698–702.
24. Sutherland I, Lindgren I. The protective effect of BCG vaccination as indicated by autopsy studies. *Tubercle*. **1979**, *60*, 225–231.
25. Kaufmann, S.H.E.; Weiner, J.; von Reyn, C.F. Novel approaches to tuberculosis vaccine development. *Int J Infect Dis.* **2017**, *56*, 263–267.
26. Whitlow, E.; Mustafa, A.S.; Hanif, S.N.M. An overview of the development of new vaccines for tuberculosis. *Vaccines* **2020**, *8*, 1–13.
27. Cardona, P.J. The progress of therapeutic vaccination with regard to tuberculosis. *Front Microbiol.* **2016**, *7*, 1–16.
28. White, A.D.; Sarfas, C.; Sibley, L.S.; Gullick, J.; Clark, S.; Rayner, E.; Gleeson, F.; Català, M.; Nogueira, I.; Cardona, P.J.; et al. Protective efficacy of inhaled BCG vaccination against ultra-low dose aerosol *M. tuberculosis* challenge in rhesus macaques. *Pharmaceutics* **2020**, *12*, 394.
29. Sibley, L.; White, A.D.; Gooch, K.E.; Stevens, L.M.; Tanner, R.; Jacobs, A.; Daykin-Pont, O.; Gleeson, F.; McIntyre, A.; Basaraba, R.; et al. High-dose *Mycobacterium tuberculosis* aerosol challenge cannot overcome BCG-induced protection in chinese origin cynomolgus macaques; implications of natural resistance for vaccine evaluation. *Sci. Rep.* **2021**, *11*, 1–14.
30. Sibley, L.; Dennis, M.; Sarfas, C.; White, A.; Clark, S.; Gleeson, F.; McIntyre, A.; Rayner, E.; Pearson, G.; Williams, A.; et al. Route of delivery to the airway influences the distribution of pulmonary disease but not the outcome of *Mycobacterium tuberculosis* infection in rhesus macaques. *Tuberculosis* **2016**, *96*, 141–149.
31. White, A.D.; Sarfas, C.; West, K.; Sibley, L.S.; Wareham, A.S.; Clark, S.; Dennis, M.J.; Williams, A.; Marsh, P.D.; Sharpe, S.A. Evaluation of the immunogenicity of mycobacterium bovis BCG delivered by aerosol to the lungs of macaques. *Clin. Vaccine Immunol.* **2015**, *22*, 992–1003.
32. Sharpe, S.A.; White, A.D.; Sibley, L.; Gleeson, F.; Hall, G.A.; Basaraba, R.J.; McIntyre, A.; Clark, S.O.; Gooch, K.; Marsh, P.D.; et al. An aerosol challenge model of tuberculosis in mauritian cynomolgus macaques. *PLoS One* **2017**, *12*, e0171906.
33. Bannister, S.; Sudbury, E.; Villanueva, P.; Perrett, K.; Curtis, N. The safety of BCG revaccination: a systematic review. *Vaccine* **2021**, *39*, 2736–2745.
34. Mahasha, P.W.; Ndwandwe, D.E.; Mavundza, E.J.; Shey, M.; Wiysonge, C.S. Systematic review protocol on bacillus Calmette-Guérin (BCG)) revaccination and protection against tuberculosis. *BMJ Open* **2019**, *9*, 1–5.
35. Lowenstine, L.J.; Osborn, K.G. Respiratory system diseases of nonhuman primates. In *Nonhuman Primates in Biomedical Research*; Elsevier Inc., 2012; pp. 413–481.
36. Peña, J.C.; Ho, W.-Z. Non-human primate models of tuberculosis. *Microbiol. Spectr.* **2016**, *4*.
37. Foreman, T.W.; Mehra, S.; Lackner, A.A.; Kaushal, D. Translational research in the nonhuman primate model of tuberculosis. *ILAR J.* **2017**, *58*, 151–159.
38. Scanga, C.A.; Flynn, J.L. Modeling tuberculosis in nonhuman primates. *Cold Spring Harb Perspect Med*. **2014,** *4*, a018564
39. Lin, P.L.; Pawar, S.; Myers, A.; Pegu, A.; Fuhrman, C.; Reinhart, T.A.; Capuano, S. V.; Klein, E.; Flynn, J.A.L. Early events in *Mycobacterium tuberculosis* infection in cynomolgus macaques. *Infect. Immun.* **2006**, *74*, 3790–3803.
40. M Langermans, J.A.; Andersen, P.; van Soolingen, D.; W Vervenne, R.A.; Frost, P.A.; van der Laan, T.; H van Pinxteren, L.A.; van den Hombergh, J.; Kroon, S.; Peekel, I.; et al. Divergent effect of bacillus Calmette-Guérin (BCG) vaccination on *Mycobacterium tuberculosis* infection in highly related macaque species: implications for primate models in tuberculosis

vaccine research. *Proc Natl Acad Sci U S A*. **2001,** *98*,11497-502.

41. Verreck, F.A.W.; Tchilian, E.Z.; Vervenne, R.A.W.; Sombroek, C.C.; Kondova, I.; Eissen, O.A.; Sommandas, V.; van der Werff, N.M.; Verschoor, E.; Braskamp, G.; et al. Variable BCG Efficacy in rhesus populations: pulmonary BCG provides protection where standard intra-dermal vaccination fails. *Tuberculosis* **2017**, *104*, 46–57.
42. Rayner, E.L.; Pearson, G.R.; Hall, G.A.; Basaraba, R.J.; Gleeson, F.; McIntyre, A.; Clark, S.; Williams, A.; Dennis, M.J.; Sharpe, S.A. Early lesions following aerosol infection of rhesus macaques (*Macaca mulatta*) with *Mycobacterium tuberculosis* strain H37RV. *J. Comp. Pathol.* **2013**, *149*, 475–485.
43. Dijkman, K.; Vervenne, R.A.W.; Sombroek, C.C.; Boot, C.; Hofman, S.O.; van Meijgaarden, K.E.; Ottenhoff, T.H.M.; Kocken, C.H.M.; Haanstra, K.G.; Vierboom, M.P.M.; et al. Disparate tuberculosis disease development in macaque species is associated with innate immunity. *Front. Immunol.* **2019**, *10*, 2479.
44. Capuano, S. V.; Croix, D.A.; Pawar, S.; Zinovik, A.; Myers, A.; Lin, P.L.; Bissel, S.; Fuhrman, C.; Klein, E.; Flynn, J.A.L. Experimental *Mycobacterium tuberculosis* infection of cynomolgus macaques closely resembles the various manifestations of human *M. tuberculosis* infection. *Infect. Immun.* **2003**, *71*, 5831–5844.
45. Maiello, P.; DiFazio, R.M.; Cadena, A.M.; Rodgers, M.A.; Lin, P.L.; Scanga, C.A.; Flynn, J.A.L. Rhesus macaques are more susceptible to progressive tuberculosis than cynomolgus macaques: a quantitative comparison. *Infect. Immun.* **2018**, *86*, e00505-17.
46. Sharpe, S.A.; Eschelbach, E.; Basaraba, R.J.; Gleeson, F.; Hall, G.A.; McIntyre, A.; Williams, A.; Kraft, S.L.; Clark, S.; Gooch, K.; et al. Determination of lesion volume by mri and stereology in a macaque model of tuberculosis. *Tuberculosis* **2009**, *89*, 405–416.
47. Sharpe, S.A.; McShane, H.; Dennis, M.J.; Basaraba, R.J.; Gleeson, F.; Hall, G.; McIntyre, A.; Gooch, K.; Clark, S.; Beveridge, N.E.R.; et al. Establishment of an aerosol challenge model of tuberculosis in rhesus macaques and an evaluation of endpoints for vaccine testing. *Clin. Vaccine Immunol.* **2010**, *17*, 1170–1182.
48. White, A.G.; Maiello, P.; Coleman, M.T.; Tomko, J.A.; Frye, L.J.; Scanga, C.A.; Lin, P.L.; Flynn, J.A.L. Analysis of 18FDG PET/CT imaging as a tool for studying *Mycobacterium tuberculosis* infection and treatment in non-human primates. *J. Vis. Exp.* **2017**.
49. Prats, C.; Vilaplana, C.; Valls, J.; Marzo, E.; Cardona, P.J.; López, D. Local inflammation, dissemination and coalescence of lesions are key for the progression toward active tuberculosis: the Bubble Model. *Front. Microbiol.* **2016**, *7*, 33.
50. Català, M.; Bechini, J.; Tenesa, M.; Pérez, R.; Moya, M.; Vilaplana, C.; Valls, J.; Alonso, S.; López, D.; Cardona, P.J.; et al. Modelling the dynamics of tuberculosis lesions in a virtual lung: role of the bronchial tree in endogenous reinfection. *PLoS Comput. Biol.* **2020**, *16*, e1007772.
51. Cardona, P.J. The key role of exudative lesions and their encapsulation: lessons learned from the pathology of human pulmonary tuberculosis. *Front. Microbiol.* **2015**, *6*, 612.
52. Cardona, P.J. A dynamic reinfection hypothesis of latent tuberculosis infection. *Infection* **2009**, *37*, 80–86.
53. Cardona, P.J. Revisiting the natural history of tuberculosis : the inclusion of constant reinfection, host tolerance, and damage-response frameworks leads to a better understanding of latent infection and its evolution towards active disease. *Arch. Immunol. Ther. Exp. (Warsz).* **2010**, *58*, 7–14.
54. Marzo, E.; Vilaplana, C.; Tapia, G.; Diaz, J.; Garcia, V.; Cardona, P.J. Damaging role of neutrophilic infiltration in a mouse model of progressive tuberculosis. *Tuberculosis* **2014**, *94*, 55–64.
55. Lin, P.L.; Maiello, P.; Gideon, H.P.; Coleman, M.T.; Cadena, A.M.; Rodgers, M.A.; Gregg, R.; O'Malley, M.; Tomko, J.; Fillmore, D.; et al. PET-CT identifies reactivation risk in cynomolgus macaques with latent *M. tuberculosis*. *PLoS Pathog.* **2016**, *12*, e1005739.
56. Hansell, D.M.; Armstrong, P.; Lynch, D.A.; McAdams, H.P. *Imaging of Diseases of the Chest*; 4th ed.; Elsevier Inc, 2005; ISBN

 doi:10.20944/preprints202211.0529.v1

0-323-03660-0-2005.

57. Webb, W.R.; Müller, N.L.; Naidich, D.P. *High-Resolution CT of the Lung*.; 3rd ed.; Lippincott Williams & Wilkins, 2003; ISBN 0-0817-2278-0-2001.
58. Leung, A.N. State-of-the-art: Pulmonary Tuberculosis. *Radiology* **1996**, *1992*, 307–322.
59. Andreu, J.; Cáceres, J.; Pallisa, E.; Martinez-Rodriguez, M. Radiological manifestations of pulmonary tuberculosis. *Eur. J. Radiol.* **2004**, *51*, 139–149.
60. Nachiappan, A.C.; Rahbar, K.; Shi, X.; Guy, E.S.; Mortani Barbosa, E.J.; Shroff, G.S.; Ocazionez, D.; Schlesinger, A.E.; Katz, S.I.; Hammer, M.M. Pulmonary tuberculosis: role of radiology in diagnosis and management. *Radiographics* **2017**, *37*, 52–72.
61. Rozenshtein, A.; Hao, F.; Starc, M.T.; Pearson, G.D.N. Radiographic appearance of pulmonary tuberculosis: dogma disproved. *Am. J. Roentgenol.* **2015**, *204*, 974–978.
62. Zeng, J.; Liu, Z.; Shen, G.; Zhang, Y.; Li, L.; Wu, Z.; Luo, D.; Gu, Q.; Mao, H.; Wang, L. MRI evaluation of pulmonary lesions and lung tissue changes induced by tuberculosis. *Int. J. Infect. Dis.* **2019**, *82*, 138–146.
63. Sharpe, S.A.; Smyth, D.; McIntyre, A.; Gleeson, F.; Dennis, M.J. Refinement and reduction through application of a quantitative score system for estimation of TB-induced disease burden using computed tomography. *Lab. Anim.* **2018**, *52*, 599–610.
64. Hislop, A.; Howard, S.; Fairweather, D.V.I. Morphometric studies on the structural development of the lung in *Macaca fascicularis* during fetal and postnatal life. *J. Anat.* **1984**, *138*, 95–112.
65. Chase, R.E. Lung Lobation in rhesus monkey, compared with man. *Amer Jour Phys Anthropol*. **1942**, *29*, 267–286.
66. Tyler, N.K.; Hyde, D.M.; Hendrickx, A.G.; Plopper, C.G. Morphogenesis of the Respiratory Bronchiole in Rhesus Monkey Lungs. *Am J Anat*. **1988**,*182*, 215-223.
67. Asgharian B, Price O, McClellan G, Corley R, Einstein DR, Jacob RE, Harkema J, Carey SA, Schelegle E, Hyde D, Kimbell JS, Miller FJ. Development of a rhesus monkey lung geometry model and application to particle deposition in comparison to humans. *Inhal Toxicol*. **2012**,24, 869-99.
68. Mercer, R.R.; Crapo, J.D. Lower respiratory tract structure of laboratory animals and humans: dosimetry implications. *Aerosol Sci. Technol.* **1993**, *18*, 257–271.
69. Hansell, D.M.; Bankier, A.A.; MacMahon, H.; McLoud, T.C.; Müller, N.L.; Remy, J. Fleischner Society: glossary of terms for thoracic imaging. *Radiology.* **2008**, *246*, 697–722.
70. Rossi, S.E.; Franquet, T.; Volpacchio, M.; Giménez, A.; Aguilar, G. Tree-in-bud pattern at thin-section CT of the lungs: radiologic-pathologic overview. *Radiographics.* **2005**, *25*, 789–801.
71. Hunter, R.L. Tuberculosis as a three-act play: a new paradigm for the pathogenesis of pulmonary tuberculosis. *Tuberculosis* **2016**, *97*, 8–17.
72. Darrah, P.A.; Zeppa, J.J.; Maiello, P.; Hackney, J.A.; Wadsworth, M.H.; Hughes, T.K.; Pokkali, S.; Swanson, P.A.; Grant, N.L.; Rodgers, M.A.; et al. Prevention of tuberculosis in macaques after intravenous BCG immunization. *Nature* **2020**, *577*, 95–102.
73. Laddy, D.J.; Bonavia, A.; Hanekom, W.A.; Kaushal, D.; Williams, A.; Roederer, M.; Seder, R.A.; Sharpe, S.A.; Verreck, F.A.W.; Darrah, P.A. Toward tuberculosis vaccine development: recommendations for nonhuman primate study design. *Infect. Immun.* **2018**, *86*, e00776-17.
74. Plumlee, C.R.; Duffy, F.J.; Gern, B.H.; Delahaye, J.L.; Cohen, S.B.; Stoltzfus, C.R.; Rustad, T.R.; Hansen, S.G.; Axthelm, M.K.; Picker, L.J.; et al. Ultra-low dose aerosol infection of mice with *Mycobacterium tuberculosis* more closely models human tuberculosis. *Cell Host Microbe* **2021**, *29*, 68-82.
75. Spertini, F.; Audran, R.; Chakour, R.; Karoui, O.; Steiner-Monard, V.; Thierry, A.-C.; Mayor, C.E.; Rettby, N.; Jaton, K.; Vallotton, L.; et al. Safety of human immunisation with a live-attenuated *Mycobacterium tuberculosis* vaccine: a randomised, double-blind, controlled phase I trial. *Lancet. Respir. Med.* **2015**, *3*, 953–962.

76. Tameris, M.; Mearns, H.; Penn-Nicholson, A.; Gregg, Y.; Bilek, N.; Mabwe, S.; Geldenhuys, H.; Shenje, J.; Luabeya, A.K.K.; Murillo, I.; et al. Live-attenuated *Mycobacterium tuberculosis* vaccine MTBVAC versus BCG in adults and neonates: a randomised controlled, double-blind dose-escalation trial. *Lancet. Respir. Med.* **2019**, *7*, 757–770.
77. Aguilo, N.; Gonzalo-Asensio, J.; Alvarez-Arguedas, S.; Marinova, D.; Gomez, A.B.; Uranga, S.; Spallek, R.; Singh, M.; Audran, R.; Spertini, F.; et al. Reactogenicity to major tuberculosis antigens absent in BCG is linked to improved protection against *Mycobacterium tuberculosis*. *Nat. Commun.* **2017**, *8*, 16085.
78. Vilaplana, C.; Marzo, E.; Tapia, G.; Diaz, J.; Garcia, V.; Cardona, P.J. Ibuprofen therapy resulted in significantly decreased tissue bacillary loads and increased survival in a new murine experimental model of active tuberculosis. *J. Infect. Dis.* **2013**, *208*, 199–202.
79. Cardona, P.J. Reactivation or reinfection in adult tuberculosis: is that the question? *Int. J. Mycobacteriology* **2016**, *5*, 400–407.
80. Hansen, S.G.; Zak, D.E.; Xu, G.; Ford, J.C.; Marshall, E.E.; Malouli, D.; Gilbride, R.M.; Hughes, C.M.; Ventura, A.B.; Ainslie, E.; et al. Prevention of tuberculosis in rhesus macaques by a cytomegalovirus-based vaccine. *Nat. Med.* **2018**, *24*, 130–143.
81. Sharpe, S.; White, A.; Sarfas, C.; Sibley, L.; Gleeson, F.; McIntyre, A.; Basaraba, R.; Clark, S.; Hall, G.; Rayner, E.; et al. Alternative BCG delivery strategies improve protection against *Mycobacterium tuberculosis* in non-human primates: protection associated with mycobacterial antigen-specific CD4 effector memory T-Cell populations. *Tuberculosis* **2016**, *101*, 174–190.
82. DiFazio, R.M.; Maiello, P.; Tomko, J.; Frye, L.; Bigbee, C.; Chedrick, C.; Updike, C.; Lin, P.; Agger, E.M.; Andersen, P.; et al. Predicting vaccine efficacy against tuberculosis using immunologic and radiologic measures in the non-human primate model (VAC7P.974). *J. Immunol.* **2014**, *192*.
83. Kraft, S.L.; Dailey, D.; Kovach, M.; Stasiak, K.L.; Bennett, J.; McFarland, C.T.; McMurray, D.N.; Izzo, A.A.; Orme, I.M.; Basaraba, R.J. Magnetic resonance imaging of pulmonary lesions in guinea pigs infected with *Mycobacterium tuberculosis*. *Infect. Immun.* **2004**, *72*, 5963–5971.